Journal of Modern Optics
Vol. 55, No. 10, 10 June 2008, 1541–1556

Taylor & Francis
Taylor & Francis Group

Downloaded By: [University of Illinois] At: 16:48 13 June 2008

Optical interferometry with pulsed fields

Robert W. Schoonover[a,b*], Brynmor J. Davis[b], Randy A. Bartels[c] and P. Scott Carney[a,b]

[a]*Department of Electrical and Computer Engineering, University of Illinois at Urbana-Champaign, Urbana, IL, USA;* [b]*The Beckman Institute for Advanced Science and Technology, University of Illinois at Urbana-Champaign, Urbana, IL, USA;* [c]*Department of Electrical and Computer Engineering, Colorado State University, Fort Collins, CO, USA*

(*Received 16 April 2007; final version received 24 September 2007*)

The problem of predicting and interpreting the results of interferometric optical experiments involving pulse trains is addressed. Specifically, a cyclostationary field arising from the modulation of a stationary, stochastic source is considered in the classical Young's experiment. It is shown that the effects of modulation may be identical to unrelated statistical interference effects.

Keywords: interferometry; metrology; statistical optics

1. Introduction

Statistical optics, or coherence theory [1], can be used to predict the outcome of measurements made with nondeterministic light. Until recently, almost all optical experiments could be well-modelled within the framework of stationary, random processes (or wide-sense stationary processes if only second order statistics, such as field intensity, are of interest). It is desirable to work within such a framework as the time-invariant nature of the statistics allows the use of powerful mathematical tools. For example, ergodicity and the Weiner–Khintchine theorem allow the meaningful interpretation of long-time-average and spectral measurements, respectively. Pulsed fields are not stationary, and must be treated within a more general theory of statistical optical fields.

Magyar and Mandel showed that when a fast-gating system is used to invalidate the usual ergodicity assumption, structure resembling interference fringes in the overlap of fields generated by independent masers may be observed, contrary to what one would expect from slow measurement systems. More recently, fast pulse generation has become the norm with pulse generation and detection being realised at the picosecond scale and faster. Furthermore, ultrafast lasers are becoming a commonplace laboratory tool to generate pulse trains. The long-time averages used in stationary theory no longer capture

*Corresponding author. Email: rschoono@uiuc.edu

ISSN 0950–0340 print/ISSN 1362–3044 online
© 2008 Taylor & Francis
DOI: 10.1080/09500340701847895
http://www.informaworld.com

Downloaded By: [University of Illinois] At: 16:48 13 June 2008

all relevant statistics, and a new formulation is required to accommodate the measurement of these pulsed fields.

An idealised optical pulse train consists of an infinite set of regularly spaced individual pulses. The spectrum for an idealised deterministic pulse train is given by the squared modulus of the Fourier transform of the field and consists of a spectral envelope, associated with a single pulse profile, modulated by a sum of delta functions regularly spaced with a period equal to the pulse repetition frequency, a so-called delta comb. Pulsed optical fields, such as those generated by mode-locked lasers, do not exist in this idealised limit and the relevant noise properties have been studied through measurements of the pulse energy on a photodiode [2–6]. Theoretical and experimental studies of photodiode radio-frequency signals produced by short laser pulses in the picosecond [7] and femtosecond regime [8–12] provide detailed information about stochastic pulse train perturbations, including timing jitter, amplitude perturbations, and pulse width fluctuations. More recently, the role of the carrier-envelope offset phase noise in spectral-comb line broadening with mode-locked few-cycle lasers has been recognised, characterised, and controlled [13–16].

The theoretical study of non-stationary statistical optics, applied to pulse trains, has seen a recent resurgence [17–20]. In the model presented in these references, a restricted class of non-stationary fields is considered in which a stationary field is modulated in a deterministic fashion – this is known as an intrinsically stationary model [21]. While this model does not encompass all pulsed optical phenomena, it is a good bridge between a general theory of non-stationary light and standard coherence theory. An intrinsically stationary model will also be used in this work to study interferometric experiments.

A unified treatment of the stochastic field fluctuations in pulsed light sources and the consequences for interferometric intensity measurements is presented. Pulses are treated as resulting from the deterministic modulation of a statistically stationary stochastic source. A mathematical model is formulated to relate observable quantities to the properties of the source. The results of this treatment demonstrate that care must be taken in the interpretation of interferograms recorded with stochastic pulsed light sources. The parameters of the deterministic modulation and the underlying stochastic source both influence the observed intensity pattern with the result that neither can be unambiguously determined from the interference pattern alone. Simulations are used to verify the mathematical model, as well as to illustrate the effects of time-varying detection.

This paper is organised as follows. In the second section, the propagation of a modulated signal is described and the two-pinhole experiment is considered. In the third section, the model is illustrated and predictions are made regarding the intensity pattern observed for various values of the system parameters. Results of simulations are shown in the fourth section, and effects of fast, time-varying detection are illustrated.

2. Modulation and propagation

In order to model a pulsed, stochastic optical field, it is natural to begin with a stationary model for the optical source and then deterministically modulate the field, so the resultant field is pulsed. The deterministic modulation functions that render the field non-stationary are not limited to those that create pulses, nor those that create statistically

Downloaded By: [University of Illinois] At: 16:48 13 June 2008

identical pulses. However, to model stable pulse generation, it is advantageous to assume each pulse is created through an identical modulation.

Consider a stochastic, statistically stationary, planar, secondary source with a mutual coherence function

$$\bar{\Gamma}_P(\boldsymbol{\rho}_1, \boldsymbol{\rho}_2, \tau) = \langle \bar{U}^*(\boldsymbol{\rho}_1, t)\bar{U}(\boldsymbol{\rho}_2, t+\tau)\rangle, \tag{1}$$

where $\bar{U}(\boldsymbol{\rho}, t)$ is the random field at position $\boldsymbol{\rho}$ and time t, and the brackets denote an ensemble average over the fluctuating scalar field. Stationarity ensures that the coherence function is not dependent on the temporal offset t. Additionally, the field is assumed to be ergodic, so the ensemble average is the same as the long time average. The Fourier transform of the mutual coherence function gives the cross-spectral density, namely,

$$\bar{W}_P(\boldsymbol{\rho}_1, \boldsymbol{\rho}_2, \omega) = \int_{-\infty}^{\infty} \mathrm{d}\tau \bar{\Gamma}_{\mathrm{P}}(\boldsymbol{\rho}_1, \boldsymbol{\rho}_2, \tau)\exp(\mathrm{i}\omega\tau). \tag{2}$$

The planar secondary source is a model, for example, for the field at one end of a laser cavity [22].

Suppose that the source is only allowed to radiate at certain times, or that the source is modulated periodically in time. The field propagated from such a system will no longer be stationary. The two-time correlation function of the nonstationary field in the source plane takes the form

$$\Gamma_{\mathrm{P}}(\boldsymbol{\rho}_1, \boldsymbol{\rho}_2, t_1, t_2) = \langle U^*(\boldsymbol{\rho}_1, t_1)U(\boldsymbol{\rho}_2, t_2)\rangle = \bar{\Gamma}_{\mathrm{P}}(\boldsymbol{\rho}_1, \boldsymbol{\rho}_2, t_2 - t_1)h^*(t_1)h(t_2), \tag{3}$$

where $U(\boldsymbol{\rho}, t) = \bar{U}(\boldsymbol{\rho}, t)h(t)$, $h(t)$ is a deterministic shutter function that describes the modulation of the source and the angled brackets denote an average over the ensemble of the underlying stationary process as in Equation (1). The bar is used to denote quantities associated with the underlying stationary field. The two-frequency cross-spectral density for the modulated field is [1]

$$\begin{aligned} W_{\mathrm{P}}(\boldsymbol{\rho}_1, \boldsymbol{\rho}_2, \omega_1, \omega_2) &= \int \mathrm{d}t_1 \mathrm{d}t_2 \Gamma_{\mathrm{P}}(\boldsymbol{\rho}_1, \boldsymbol{\rho}_2, t_1, t_2)\exp[\mathrm{i}(\omega_2 t_2 - \omega_1 t_1)] \\ &= \int \frac{\mathrm{d}\beta}{2\pi} H^*(\omega_1 - \beta)H(\omega_2 - \beta)\bar{W}_{\mathrm{P}}(\boldsymbol{\rho}_1, \boldsymbol{\rho}_2, \beta), \end{aligned} \tag{4}$$

where, again, the bar denotes the cross-spectral density of the underlying stationary source and $H(\omega)$ is the Fourier transform of $h(t)$. The convolution has the effect of broadening the spectrum of the underlying process.

In an ideal pulse train, each pulse is deterministic and identical. However, because of noise processes in the system, this is generally not realisable. Within this work, the pulses are *statistically* identical if the deterministic modulation/shutter is chosen to be periodic

$$h(t) = \sum_{n=1}^{N} h_{\mathrm{p}}(t - nT_0), \tag{5}$$

where $h_{\mathrm{p}}(t)$ is the deterministic modulation for a single pulse. This periodic form of modulation results in a field that is cyclostationary for $N \to \infty$ [23,24]. Cyclostationarity

Downloaded By: [University of Illinois] At: 16:48 13 June 2008

and cyclo-ergodicity are well explored concepts in signal processing, resulting in a significant body of literature which can be leveraged in studying non-deterministic, pulsed optical fields [25]. The form of $h_{\mathrm{p}}(t)$ can be chosen to model pulse shape, chirp, and other deterministic effects. The cross-spectral density takes the form

$$W_{\mathrm{P}}(\boldsymbol{\rho}_1, \boldsymbol{\rho}_2, \omega_1, \omega_2) = \sum_{m=1}^{N}\sum_{n=1}^{N} \exp[\mathrm{i}T_0(m\omega_2 - n\omega_1)] \times \int \frac{\mathrm{d}\beta}{2\pi} H_{\mathrm{p}}^{*}(\omega_1 - \beta) H_{\mathrm{p}}(\omega_2 - \beta) \bar{W}_{\mathrm{P}}(\boldsymbol{\rho}_1, \boldsymbol{\rho}_2, \beta) \times \exp[-\mathrm{i}T_0\beta(m-n)]. \tag{6}$$

This result differs from other reported works [17–19] in that the whole train of pulses is considered rather than assuming that each pulse is incoherent with all other pulses. The spectral density [19] of the pulsed beam as a function of frequency and position is defined to be

$$S(\boldsymbol{\rho}, \omega) = W_{\mathrm{P}}(\boldsymbol{\rho}, \boldsymbol{\rho}, \omega, \omega) = \int \frac{\mathrm{d}\beta}{2\pi} \bar{W}_{\mathrm{P}}(\boldsymbol{\rho}, \boldsymbol{\rho}, \omega - \beta) |H_{\mathrm{p}}(\beta)|^2 \sum_{m=1}^{N}\sum_{n=1}^{N} \exp[\mathrm{i}T_0(m-n)\beta]. \tag{7}$$

This quantity represents the energy present at frequency ω at position $\boldsymbol{\rho}$. It can be seen that as N becomes large, the double summation converges to a delta comb with a period of $2\pi/T_0$. The comb is modulated by the spectrum of a single pulse before being convolved with the cross-spectral density of the underlying stationary source. Equation (7) can be seen to correspond to the conventional understanding of the frequency comb – the comb period is the pulse repetition frequency, the duration of a single pulse determines the width of the comb and non-deterministic effects broaden the line width.

The model presented in this paper represents a stochastic pulsed field as a modulated stationary optical field. The underlying stochastic field is assumed to have a coherence time τ_{c}, the duration of the single pulse $h_{\mathrm{p}}(t)$ is characterised by T and the pulses are repeated with a period T_0. The relationship between these three time scales (T_0, T, and τ_{c}) determines the statistical properties of the pulsed field. Pulsed fields can be readily classified into several distinct regimes based on these parameters. Three of these regimes cover most physically realisable experiments.

- Regime I is defined by $T < T_0 \ll \tau_{\mathrm{c}}$. In this regime pulses separated by several T_0 exhibit significant correlations. This regime includes devices such as stable mode-locked lasers with long-term fluctuations in the pulse properties, which may include timing jitter, amplitude fluctuations, carrier-envelope phase fluctuations, etc. In this regime non-deterministic behavior results in a modest broadening of spectral comb lines [2]. In terms of Equation (7), the width of $\bar{W}_{\mathrm{P}}(\boldsymbol{\rho}_1, \boldsymbol{\rho}_2, \omega)$ is less than the comb spacing $2\pi/T_0$, so the comb structure remains, albeit with a broader line width.
- Regime II is defined by $T < \tau_{\mathrm{c}} < T_0$, where pulses separated by the pulse period T_0 may exhibit a significant statistical relationship, but pulses separated by multiple repetition periods are statistically uncorrelated. Highly unstable mode-locked lasers may operate in this regime. Here one expects the power spectral density to be

Downloaded By: [University of Illinois] At: 16:48 13 June 2008

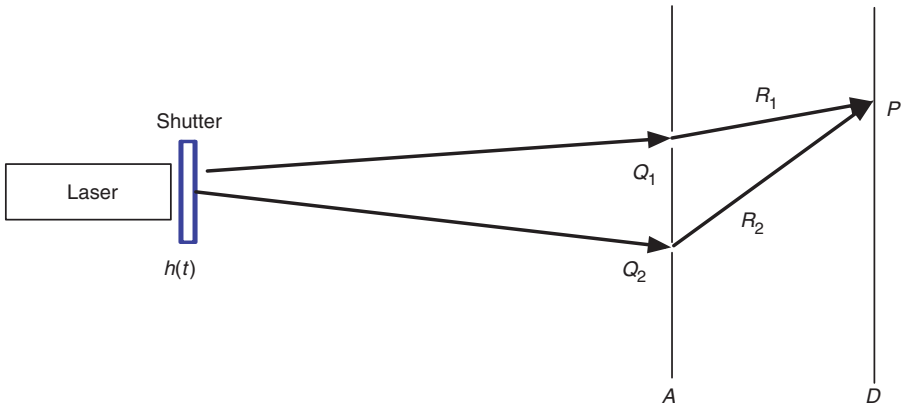

Figure 1. A diagrammatic sketch of the pulsed system.

continuous as the spectral width of the underlying stationary field approaches the repetition frequency $\omega_r = 2\pi/T_0$ of the pulsed light field. However, the bandwidth of the signal is still determined by the pulse duration T.

- Regime III is defined by $\tau_c \ll T < T_0$, the so-called continuous-wave limit [26]. In this regime, the pulses are separated by significantly more than τ_c and so the fields in separate pulses are not statistically related. Additionally, the condition $\tau_c \ll T$ indicates that the field at the beginning of a pulse is statistically uncorrelated with the field at the end of the pulse. The power spectral density in this regime is dominated by that of the underlying stochastic field. The convolution with $\bar{W}_P(\boldsymbol{\rho}_1, \boldsymbol{\rho}_2, \omega)$ in Equation (7) destroys the comb structure and spreads the spectrum beyond the limits of the deterministic pulse.

Returning to the propagation and interference of pulsed fields, a Young's two-pinhole experiment is shown in Figure 1 and is similar to many experiments such as that described in [27]. The pulsed field is propagated to a screen $\mathcal{A}$ that includes two pinhole apertures. The screen $\mathcal{A}$ is chosen to be perpendicular to the direction of propagation and a distance z away from the shutter. The output of the Young's two-pinhole experiment is then measured at a detector in the plane $\mathcal{D}$, parallel to $\mathcal{A}$.

The cross-spectral density satisfies a double reduced wave equation and so may be propagated by the method of Green functions. It has been shown [19] that the cross-spectral density for the propagated field $U_S(\boldsymbol{r}, \omega)$ satisfies the equation

$$(\nabla_1^2 + k_1^2)(\nabla_2^2 + k_2^2) W_S(\boldsymbol{r}_1, \boldsymbol{r}_2, \omega_1, \omega_2) = (4\pi)^2 W_Q(\boldsymbol{\rho}_1, \boldsymbol{\rho}_2, \omega_1, \omega_2), \tag{8}$$

where $k_i = w_i/c$ and W_Q is the cross-spectral density of the primary source. This result implies that the cross-spectral density for the field radiated by a secondary, planar source is given by the expression

$$W_S(\boldsymbol{r}_1, \boldsymbol{r}_2, \omega_1, \omega_2) = \frac{1}{(2\pi)^2} \iint_{z'=0} \mathrm{d}^2\rho_1' \mathrm{d}^2\rho_2' W_P(\boldsymbol{\rho}_1', \boldsymbol{\rho}_2', \omega_1, \omega_2) \times \frac{\partial}{\partial z_1'} \frac{\partial}{\partial z_2'} \frac{\exp(-\mathrm{i}k_1|\boldsymbol{r}_1 - \boldsymbol{r}_1'|)}{|\boldsymbol{r}_1 - \boldsymbol{r}_1'|} \frac{\exp(\mathrm{i}k_2|\boldsymbol{r}_2 - \boldsymbol{r}_2'|)}{|\boldsymbol{r}_2 - \boldsymbol{r}_2'|}, \tag{9}$$

Downloaded By: [University of Illinois] At: 16:48 13 June 2008

where W_S is the cross-spectral density for the field U_S and W_P is the cross-spectral density for the secondary source. When the source is of uniform spatial intensity in the entire plane and there is complete spatial coherence among all pairs of points in the plane, the propagated field is a polychromatic plane wave with the same spectral content as the source.

At a point P on the detection screen (see Figure 1), the ensemble average of the instantaneous intensity as a function of time is related to the fields in the two pinholes by the equation

$$\begin{aligned}\Gamma_{\mathcal{D}}(P,P,t,t) = {} & |K_1|^2\Gamma_{\mathcal{A}}(Q_1,Q_1,t-R_1/c,t-R_1/c)\\ & + |K_2|^2\Gamma_{\mathcal{A}}(Q_2,Q_2,t-R_2/c,t-R_2/c)\\ & + K_1^*K_2\Gamma_{\mathcal{A}}(Q_1,Q_2,t-R_1/c,t-R_2/c)\\ & + K_1K_2^*\Gamma_{\mathcal{A}}(Q_2,Q_1,t-R_2/c,t-R_1/c),\end{aligned} \tag{10}$$

where the K_i are constant factors that depend on the area of the holes and the distance R_i from the ith pinhole to the point P (see Figure 1). When the bandwidth is narrow, $K_i = -\mathrm{i}\mathrm{d}\mathcal{A}/\bar{\lambda}R_i$ [28], where $\bar{\lambda} = 2\pi c/\omega_c$ and $\mathrm{d}\mathcal{A}$ is the area of the pinhole. By mapping the delay $t_d = (R_2 - R_1)/c$ to points P on the plane, one can construct the expected intensity pattern at the detector, or conversely, determine temporal coherence properties from such a measurement.

3. Interferometric measurement

Consider a specific example of a pulsed field that is created by modulating a stationary, random process. The cross-spectral density of the stationary laser source is taken to be

$$\bar{W}_P(\boldsymbol{\rho}_1,\boldsymbol{\rho}_2,\omega) = \exp\left(-\frac{(\omega-\omega_c)^2}{2\sigma^2}\right), \tag{11}$$

where σ defines the effective bandwidth of the source and ω_c is the center frequency of the light. Notice that this planar stationary source is spatially completely coherent in the sense that the spectral degree of coherence is of unit magnitude. The shutter function is likewise taken to be a Gaussian with effective pulse time T, namely,

$$h_p(t) = \exp\left(-\frac{t^2}{2T^2}\right). \tag{12}$$

These pulses are the so-called Gaussian–Schell model pulses [17].

When T_0 is much larger than $\tau_c \approx 1/\sigma$ and T (i.e. regimes II and III), only fields within individual pulses exhibit a non-zero correlation. Thus, the overlap at the screen between pulses can be ignored and $h_p(t)$ can replace $h(t)$ in the calculation. An additional simplification, that the fractional bandwidth σ/ω_c is sufficiently small, and some calculation yields the normalized mutual coherence function at the screen $\mathcal{A}$,

$$\Gamma_{\mathcal{A}}(z,z,t,t+t_d) = \exp\left[-\frac{(2t+t_d-2z/c)^2}{4T^2}\right]\exp\left[-\frac{t_d^2}{2\Delta^2}\right]\exp(-\mathrm{i}\omega_c t_d), \tag{13}$$

Downloaded By: [University of Illinois] At: 16:48 13 June 2008

where

$$\Delta^2 = \frac{2T^2}{1+2\sigma^2T^2}, \\ = \frac{2T^2\tau_c^2}{\tau_c^2+2T^2}. \tag{14}$$

Note that in regime III, Equation (14) is approximated by taking $\Delta^2 \approx \tau_c^2$, i.e. the autocorrelation is dominated by the properties of the underlying stationary stochastic field. In regime I $\Delta^2 \approx 2T^2$ and the autocorrelation is then dominated by the effect of the pulsed modulation.

Any real measurement of the intensity at the detector involves an integration over the time, t. By assuming that the order of the temporal integration and the expectation operator can be interchanged, the expected measurement can be found by integrating Equation (10) over all time. The expected normalized detector-integrated intensity pattern on the screen can be shown to be

$$I(P) = \int_{-\infty}^{\infty} \mathrm{d}t \Gamma_{\mathcal{D}}(P,P,t,t) \propto 1 + \exp(-t_d^2/2\Delta^2)\cos(\omega_c t_d), \tag{15}$$

where t_d is the difference in propagation times from the two pinholes, i.e. $t_d = (R_2 - R_1)/c$. In order to achieve a stable, meaningful measurement, the variance of $I(P)$ about its mean must go to zero, i.e. an ergodicity condition is required [25]. In deriving Equation (15), slow detection was assumed, i.e. the detector integration time is much larger than any other time scale in the system. If the slow detector integration time greatly exceeds T_0, the interference pattern will not change in time, as the diffraction patterns from individual pulse members are statistically unrelated.

Plots of the detector-integrated intensity are shown in Figures 2 and 3. In Figure 2, the shape of the interferogram is mainly determined by the coherence time ($\tau_c \approx 1/\sigma$). The pulse time, T, is not a factor in the interference pattern (although it affects the total recorded intensity). In Figure 3, the shape of the interferogram is mainly determined by the pulse time, T. Despite the fact that the two figures represent fields in two separate regions of the parameter space, the resultant integrated intensity patterns are nearly indistinguishable at the detector. This result implies that an interferometric measurement cannot distinguish between coherence time of the original pulse and the shaping of that pulse through $h(t)$. Such an ambiguity mirrors one shown in the spectral domain in which fields that lie in different regimes of parameter space can have identical spectra [17].

Now consider the interference pattern produced when interference between multiple pulses may be recorded, i.e. regime I. Similar calculations yield the intensity on the screen after many pulses,

$$I(P) = 1 + \sum_n \sum_m \exp\left(-\frac{(m-n)^2 T_0^2 \sigma^2}{2+4\sigma^2T^2}\right) \\ \times \exp\left[-\frac{\Delta^2}{2}\left(\frac{t_d}{\Delta^2} + \frac{(m-n)T_0}{2T^2}\right)^2\right]\cos(\omega_c t_d). \tag{16}$$

Downloaded By: [University of Illinois] At: 16:48 13 June 2008

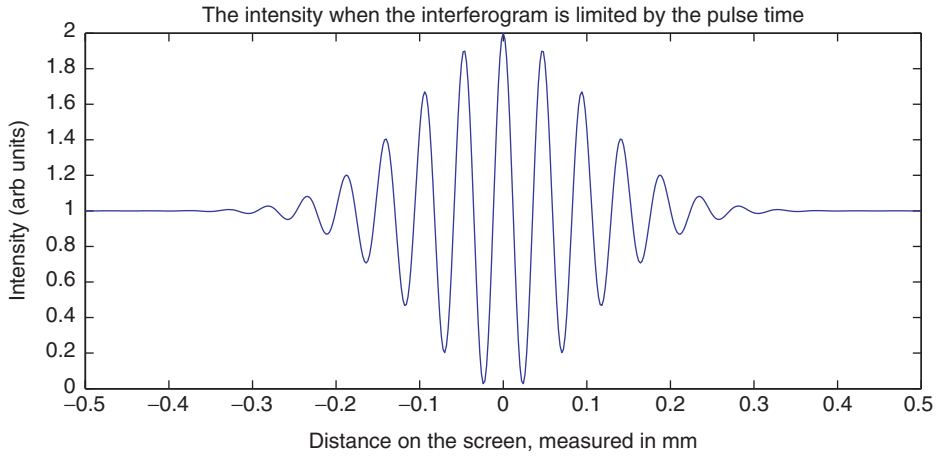

Figure 2. The interference pattern for a field with $\omega_c = 10^{15}\,\mathrm{rad\,s^{-1}}$, $T = 10\,\mathrm{fs}$, $\tau_c = 1/\sigma = 100\,\mathrm{fs}$, and $T_0 \gg \tau_c, T$, i.e. regime II. In this example, the pulse time is the dominant parameter, as the coherence time is 10 times greater. Here, and in all other simulations, the distance between planes $\mathcal{A}$ and $\mathcal{D}$ is $d = 50\,\mathrm{mm}$ and the spacing between the slits is 2 mm.

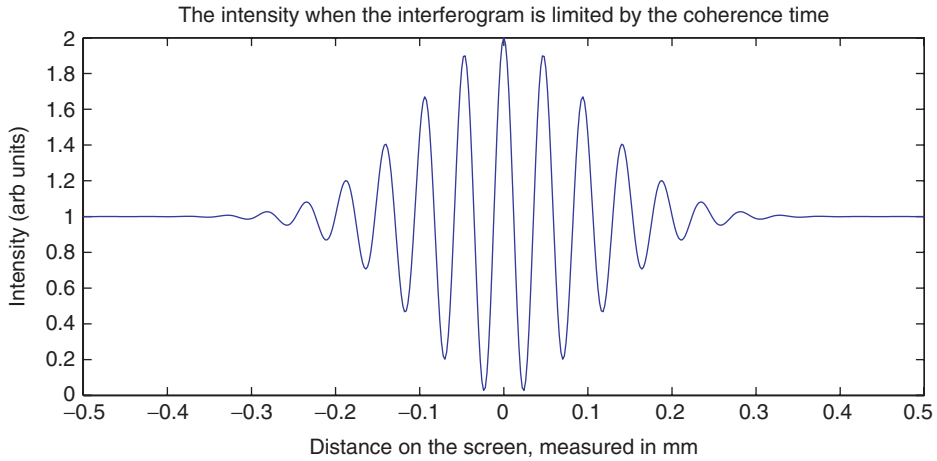

Figure 3. The interference pattern for a field with $\omega_c = 10^{15}\,\mathrm{rad\,s^{-1}}$, $T = 50(2^{1/2})\,\mathrm{fs}$, $\tau_c = 1/\sigma = 10(2^{1/2})\,\mathrm{fs}$ and $T_0 \gg \tau_c, T$, i.e. regime III. In this example, the coherence time is the dominant parameter, as the pulse time is 5 times greater.

This equation is valid as long as consecutive pulses do not overlap, i.e. when $T_0 > T$. It is noteworthy that consecutive pulses may create secondary interference patterns on the screen spaced, in delay time, by multiples of the pulse period T_0. The primary interference pattern, occurring when $n = m$, represents the superposition of correlated fields within individual pulses. The secondary interference structures are due to the cross-correlation between the fields in pulses $m \neq n$, where $T_0|m - n|$ is the time delay between the two pulses. The number of the secondary interference patterns is dictated by the relevant regime. In regime I, since the coherence time extends across multiple pulses, approximately

Downloaded By: [University of Illinois] At: 16:48 13 June 2008

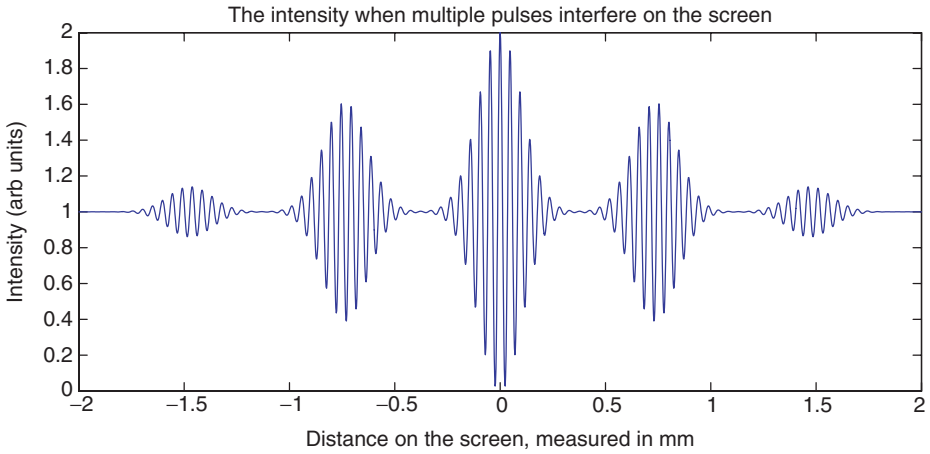

Figure 4. The interference pattern for a field with $\omega_c = 10^{15}\,\mathrm{rad\,s^{-1}}$, $T = 10\,\mathrm{fs}$, $\tau_c = 1/\sigma = 100\,\mathrm{fs}$, and $T_0 = 100\,\mathrm{fs}$, i.e. regime I. In this example, the coherence time is the dominant parameter, as the pulse duration is 10 times smaller than the coherence time. Multiple pulses can be seen to interfere on the screen. Note that $\pm$ 0.75 mm on the screen corresponds to a delay of 100 fs.

τ_c/T_0 secondary interference structures will be present in the interference pattern. In regimes II and III, only the primary interference structure will be present. In these cases, the secondary interference patterns wash out with time-averaging because the fields in consecutive pulses are incoherent. In Figure 4, an interferogram is shown with the same properties as Figure 2, only with T_0 now small enough that consecutive pulses are within the coherence time of each other. One can see that smaller interference patterns show up next to the standard interference pattern in the center. The case that $\tau_c > T_0$ shows that consecutive pulses can have a stable phase relation and hence produce predictable interference fringes. The repetition rate ($1/T_0$) is beyond what is currently realisable, but was chosen to show interpulse interference effects. Typical ultrafast pulsed lasers operate with repetition rate frequencies from tens of MHz to tens of GHz. However, a harmonically mode-locked diode laser has been demonstrated to operate at 500 GHz [29] ($T_0 = 2$ ps), which is similar to the values used in these simulations and is likely sufficient to observe interpulse effects.

The utility of a two-pinhole interferometer lies in the fact that the position on the screen maps directly to the time-difference coordinate. However, in the non-stationary case, the mutual correlation function depends also on an absolute time coordinate. The dependence on the absolute time coordinate reflects the fact that the deterministic pulse modulates the stationary stochastic field. Each pulse in the pulse train generates a distinct diffraction pattern and the correlation that one might naively deduce from individual diffraction patterns (i.e. modulus squared of the diffracted field) is not equivalent to the statistical correlation that one recovers with sufficient averaging. Time averaging by slow detectors effectively projects the mutual coherence onto the screen without any resolution of the absolute time coordinate. Even fast detectors can only approximately resolve the dependence on the absolute time coordinate, with a resolution determined on the integration time of the detector. Thus, the absolute time-dependence in Γ is often lost when performing an interference experiment. Without knowledge of the

Downloaded By: [University of Illinois] At: 16:48 13 June 2008

dependence on both time variables, one can no longer use Fourier transform relations to unambiguously map the spectrum [see Equation (7)] to the detected intensity [see Equation (16)]. Information regarding pulse duration, stability and repetition rate is now mixed in an underdetermined fashion and thus T, T_0, and τ_c cannot be resolved uniquely.

4. Simulations and discussion

Results from the previous section for average quantities can be verified through numerical simulations of realisations of the random field. In particular, simulations show that time-averaged measurements coincide with the predicted measurements, validating the assumption of cyclo-ergodicity used in Equation (15). Following the strategy presented in [30], realisations of a discrete random process are used to simulate the source. A complex, white, Gaussian random process is realized using a random number generator and then fed into a linear shift-invariant filter so that the output random process has the spectrum given in Equation (11). This process is then modulated to produce a pulsed field. The signal at a given point on the screen, neglecting propagation factors, can then be found by taking two copies of the field, offsetting each in time by an amount corresponding to the pinhole-to-screen distance, and taking the square magnitude of their sum. The result gives the intensity on the screen as a function of time and with a temporal resolution higher than what is currently achievable experimentally. A time average is then implemented to simulate measurable quantities.

In these simulations, pulses are created by realising the underlying stationary process $\bar{U}(t)$. Simulations of the scenarios shown in Figures 2, 3 and 4 are shown in Figures 5, 6 and 7, respectively. There is good agreement between the simulations and the analytic results. The instantaneous intensity is shown as a function of screen position and time in the upper plot, and the time average as a function of position is shown in the lower plot. These simulations provide an alternative numerical means to calculate measurable quantities at the screen. One can also attain representative fields that are accessible neither via measurement nor through analytic calculations based only on second-order statistics. The intensity of such a representative field is shown in the upper plots of Figures 5, 6 and 7. One notices that each pair of overlapping pulses produces an oscillatory intensity pattern, but these should not be confused with interference patterns. Magyar and Mandel showed previously that uncorrelated light can create diffraction patterns that look like interference [31], but as they rightly concluded, this is not a statistical effect. As seen in the figures, many of these features wash out due to instability in the fringe position. Only the fields displaying coherence (or at least partial coherence) have the stable phase structure that allows the oscillations to survive the time averaging.

The necessity of taking long-time averages to get stable, statistically meaningful results requires taking averages over many pulses. As an example of what may happen when too little data is taken, in Figure 8 a plot of the integrated intensity averaged over two pulses is shown. The two-pulse average is very clearly different than the 500-pulse measurements shown in Figure 6 with the same system parameters. It is clear that any measurement averaged over only a few pulses will not be indicative of the underlying random process associated with the pulsed field.

Downloaded By: [University of Illinois] At: 16:48 13 June 2008

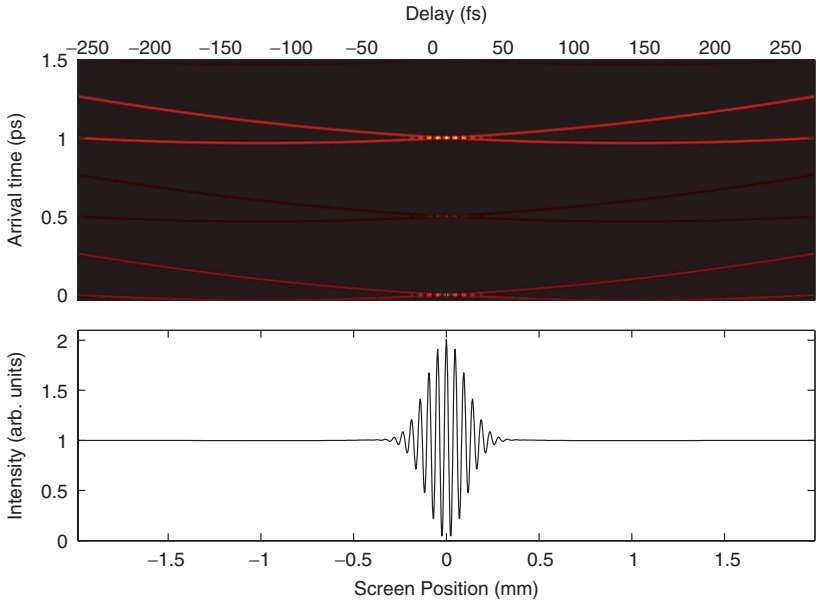

Figure 5. A simulation with $T = 10\,\text{fs}$, $T_0 = 500\,\text{fs}$, $\tau_c = 100\,\text{fs}$ and $\omega_c = 10^{15}\,\text{rad}\,\text{s}^{-1}$ with 100 pulses measured. The top plot shows the instantaneous intensity as a function of screen position and time. Note that only a small fraction of the time axis is shown. The bottom plot is the average of the signal over the full 100 pulses. See Figure 2 for analytic results. (The colour version of this figure is included in the online version of the journal.)

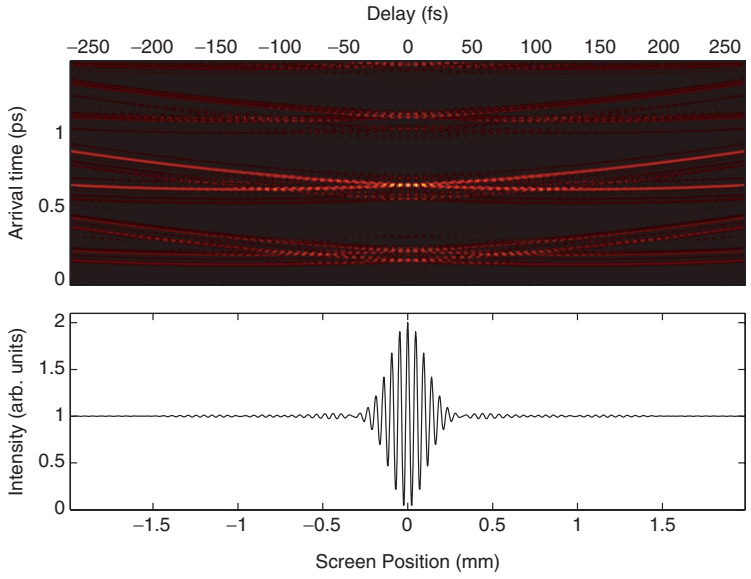

Figure 6. A simulation with $T = 50(2^{1/2})\,\text{fs}$, $T_0 = 500\,\text{fs}$, $\tau_c = 10(2^{1/2})\,\text{fs}$ and 100 pulses are again measured. Speckle-like effects, where different parts of the pulse interfere with each other are visible in the upper plot. There is only phase-stability around the coherence length. See Figure 3 for analytic results. (The colour version of this figure is included in the online version of the journal.)

Downloaded By: [University of Illinois] At: 16:48 13 June 2008

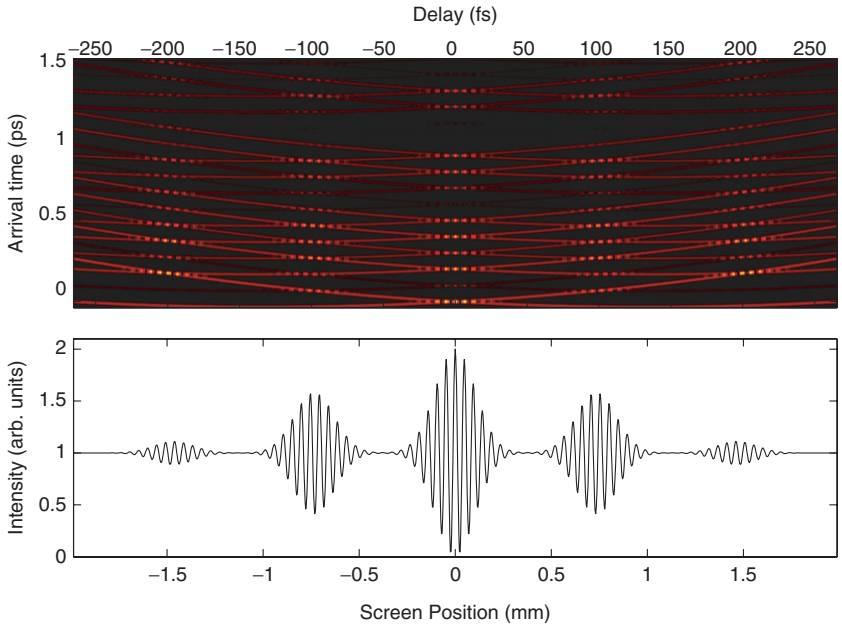

Figure 7. A simulation with the parameters $T = 10\,\text{fs}$, $T_0 = 100\,\text{fs}$, $\tau_c = 100\,\text{fs}$ and 500 pulses measured. The interpulse interference is stable; secondary fringe structures are thus present. See Figure 4 for analytic results. (The colour version of this figure is included in the online version of the journal.)

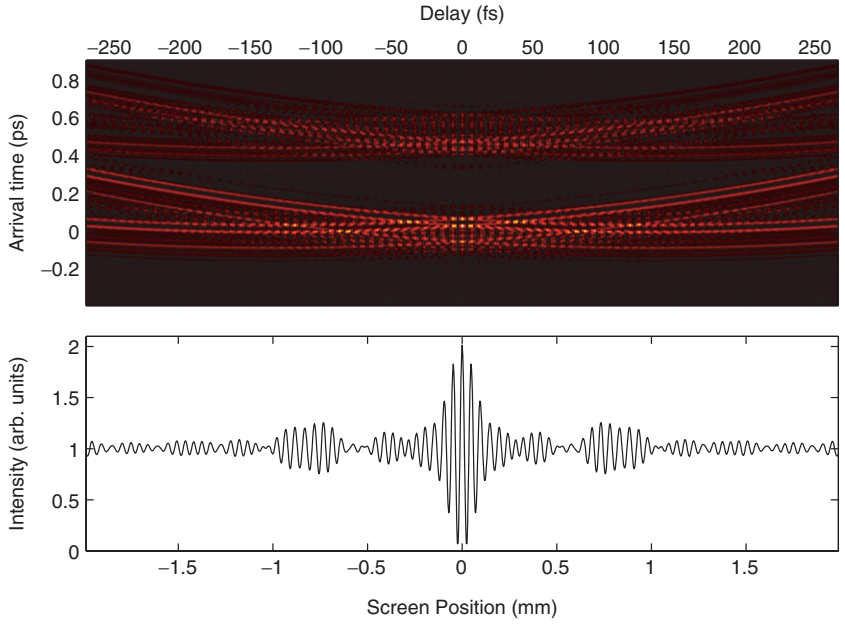

Figure 8. A simulation with system parameters $T = 100\,\text{fs}$, $\tau_c = 10\,\text{fs}$, $T_0 = 500\,\text{fs}$ and only two pulses measured. The measured intensity has not converged to its many-pulse average. (The colour version of this figure is included in the online version of the journal.)

Downloaded By: [University of Illinois] At: 16:48 13 June 2008

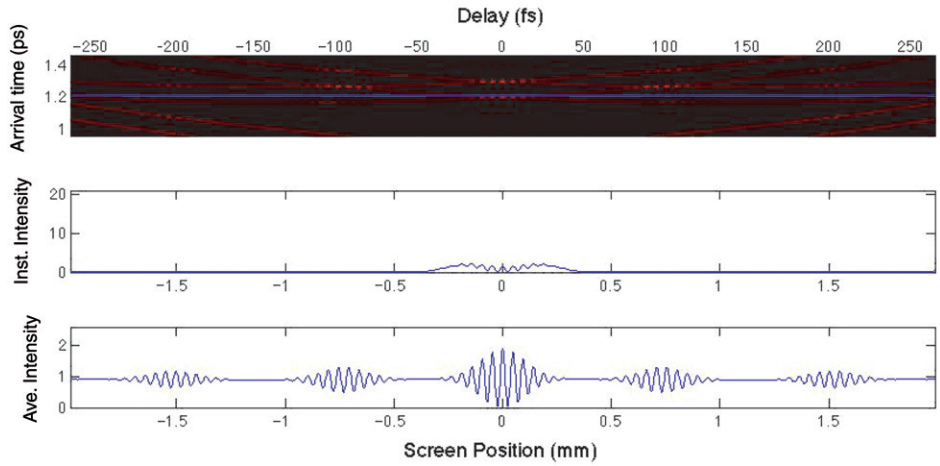

Figure 9. A simulation with system parameters $T = 10\,\text{fs}$, $\tau_c = 500\,\text{fs}$, $T_0 = 100\,\text{fs}$. The top panel shows the optical intensity as a function of time or screen position after passing through the two pinholes. The blue line running across this panel represents the detection plane. The second panel shows the instantaneous intensity, not $\Gamma(P, P, t, t)$, of the field as a function of position. The third panel shows the accumulated average intensity. In this simulation, one notices a stable instantaneous fringe position which results in several measurable fringe patterns in the average intensity. (The colour version of this figure is included in the online version of the journal.)

In Figure/movie 9, a simulation of a random field (with system parameters characteristic of regime I) impinging on the detector is shown. Again, one can see fringes in the instantaneous intensity, and due to a long coherence time, these fringes remain stable across the detection screen. Consecutive pulses fall within the coherence time of the field, and multiple interference patterns appear at the detector.

In Figure/movie 10, the simulation shown is characteristic of regime II. The system parameters are the same as in Figure 9 excepting the coherence time, which is significantly shorter. Even though consecutive pulses overlap on the detector, producing fringes in the plot of instantaneous intensity, these are not phase-stable due to the short coherence time.

These simulations make clear the fact that measures of coherence must be taken over long times, which is to say, many pulses. Recently, experiments to measure the coherence properties of short pulses have appeared in the literature. In some cases, the coherence properties are measured over many pulses [27]. In others, single- or few-shot measurements are made [32, 33]. In both these cases, however, the pulse time T is much longer than the coherence time τ_c. This effectively accounts for the time-averaging needed when shorter pulses are employed.

Both the simulation of fields in Figures 5–7 and the mathematical descriptions of the average intensity in Equation (15) assume long detection times. Often, however, measurements are made with time-gated systems to reduce noise. The theory presented in this work can easily be extended to such cases by altering the form of Equation (15) to account for the change in detection time, namely,

$$\int_{-\infty}^{\infty} \mathrm{d}t \rightarrow \int_{-\infty}^{\infty} \mathrm{d}t\, h_{\mathrm{d}}(t), \tag{17}$$

Downloaded By: [University of Illinois] At: 16:48 13 June 2008

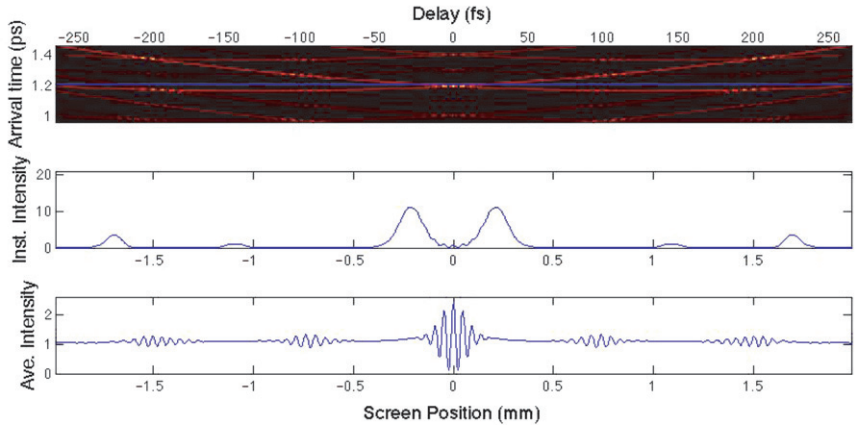

Figure 10. A simulation with system parameters $T = 10\,\text{fs}$, $\tau_c = 10\,\text{fs}$, $T_0 = 100\,\text{fs}$. In the simulation above, one notices a similar instantaneous intensity pattern. However, the fringe position is not stable except in a region near $x = 0$, as can be seen by the lack of fringes off-centre in the plot of final accumulated intensity. Running this simulation for longer than is presented will further reduce the secondary fringes to a negligible level (cf. Figures 6). (The colour version of this figure is included in the online version of the journal.)

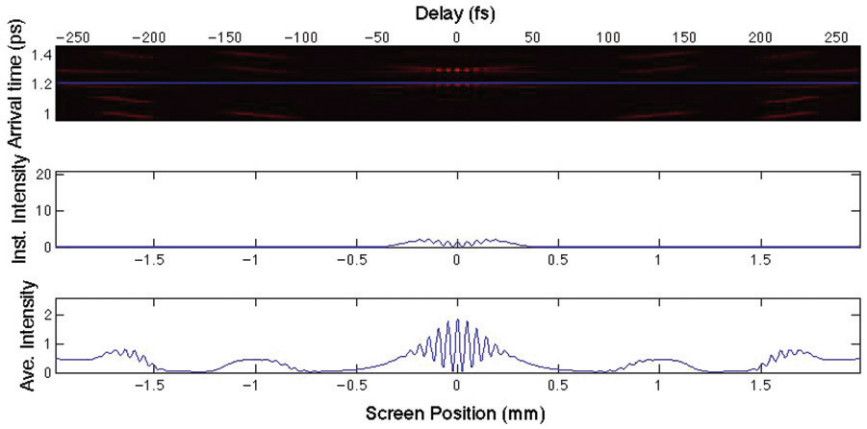

Figure 11. A simulation with system parameters $T = 10\,\text{fs}$, $\tau_c = 100\,\text{fs}$, $T_0 = 100\,\text{fs}$ and a gated detector with repetition period equal to T_0 and a gate-width of 40 fs. One can see that parts of the wavefronts are no longer detected as shown in the top two plots. In the upper plot, the part of the field that is not detected no longer appears in the spatio-temporal representation of the field intensity. Since each screen position corresponds to different arrival times of the field, the gated detection results in intensity nulls (seen at $\pm 0.6\,\text{mm}$ and $\pm 1.4\,\text{mm}$). One can compare the final frame of this movie to Figure 7 to see the difference between slow detection and fast, gated detection. (The colour version of this figure is included in the online version of the journal.)

where $h_d(t)$ can account for time-gating. Care needs to be taken that cyclo-ergodicity constraints are still met in such detection. As one can see in Figure/movie 11, the process of gated detection can significantly alter the interferogram created by a pulsed field. One can compare Figure 11 to Figure 7 to see the difference in gated detection, since both

Downloaded By: [University of Illinois] At: 16:48 13 June 2008

simulations use the same temporal parameters for the pulsed field. One can also include in this model the process of 'physical detection' by adding in another term in the integrand of Equation (15) to account for the frequency response of the detector [34].

5. Conclusion

The interference pattern in a Young's two-pinhole experiment has been examined in the context of pulsed, stationary fields. Three time scales are important in such fields: the coherence time, the pulse time, and the interpulse time. Based on these time scales, regimes have been identified to classify the interferograms generated by these pulses. Analytic results illustrate an equivalence between interferograms from different regimes and predict multipulse interference effects. Numerical simulations verify these results, and also illustrate the role of gated detection in interpreting interferograms for pulsed fields. The two-pinhole interferometer used in this paper could equally well be replaced with a Michelson interferometer or a number of other interferometric detection devices.

Acknowledgements

RWS, BJD and PSC acknowledge support by the National Science Foundation under CAREER Grant No. 0239265. RAB acknowledges support from the National Science Foundation under Award ECS-0348068 and support from a Sloan Research Fellowship.

References

[1] Mandel, L.; Wolf, E. *Optical Coherence and Quantum Optics;* Cambridge University Press: Cambridge, UK, 1995.
[2] Vonderlinde, D. *Appl. Phys. B* **1986,** *39* (4), 201–217.
[3] Haus, H.A.; Mecozzi, A. *IEEE J. Quantum Electron.* **1993,** *29* (3), 983–996.
[4] Fuss, I.G. *IEEE J. Quantum Electron.* **1994,** *30* (11), 2707–2710.
[5] Eliyahu, D.; Salvatore, R.A.; Yariv, A. *J. Opt. Soc. Am. B* **1996,** *13* (7), 1619–1626.
[6] Eliyahu, D.; Salvatore, R.A.; Yariv, A. *J. Opt. Soc. Am. B* **1997,** *14* (1), 167–174.
[7] Leep, D.A.; Holm, D.A. *Appl. Phys. Lett.* **1992,** *60* (20), 2451–2453.
[8] Spence, D.E.; Evans, J.M.; Sleat, W.E.; Sibbett, W. *Opt. Lett.* **1991,** *16* (22), 1762–1764.
[9] Son, J.; Rudd, J.V.; Whitaker, J.F. *Opt. Lett.* **1992,** *17* (10), 733–735.
[10] Spence, D.E.; Dudley, J.M.; Lamb, K.; Sleat, W.E.; Sibbett, W. *Opt. Lett.* **1994,** *19* (7), 481–483.
[11] Aoyama, M.; Yamakawa, K. *Opt. Commun.* **1997,** *140* (4–6), 255–258.
[12] Poppe, A.; Xu, L.; Krausz, F.; Spielmann, C. *IEEE J. Quantum Electron.* **1998,** *4* (2), 179–184.
[13] Xu, L.; Spielmann, C.; Poppe, A.; Brabec, T.; Krausz, F.; Hansch, T.W. *Opt. Lett.* **1996,** *21* (24), 2008–2010.
[14] Jones, D.J.; Diddams, S.A.; Ranka, J.K.; Stentz, A.; Windeler, R.S.; Hall, J.L.; Cundiff, S.T. *Science* **2000,** *288* (5466), 635–639.
[15] Holman, K.W.; Jones, R.J.; Marian, A.; Cundiff, S.T.; Ye, J. *Opt. Lett.* **2003,** *28* (10), 851–853.
[16] Matos, L.; Mucke, O.D.; Chen, J.; Kartner, F.X. *Opt. Express* **2006,** *14* (6), 2497–2511.
[17] Lajunen, H.; Tervo, J.; Turunen, J.; Vahimaa, P.; Wyrowski, F. *Opt. Express* **2003,** *11* (16), 1894–1899.
[18] Lajunen, H.; Tervo, J.; Vahimaa, P. *J. Opt. Soc. Am. A* **2004,** *21* (11), 2117–2123.
[19] Lajunen, H.; Vahimaa, P.; Tervo, J. *J. Opt. Soc. Am. A* **2005,** *22* (8), 1536–1545.

Downloaded By: [University of Illinois] At: 16:48 13 June 2008

[20] Torres-Company, V.; Lajunen, H.; Friberg, A.T. *J. Eur. Opt. Soc. Rapid Pub.* **2007,** *2*, 07007-1–4.
[21] Gase, R.; Schubert, M. *J. Mod. Opt.* **1982,** *29* (10), 1331–1347.
[22] Wolf, E.; Agarwal, G.S. *J. Opt. Soc. Am. A* **1984,** *1*, 541–546.
[23] Yaglom, A.M. *Correlation Theory of Stationary and Related Random Functions;* Springer: Berlin, 1987.
[24] Gardner, W.A.; Napolitano, A.; Paura, L. *Signal Process.* **2006,** *86* (4), 639–697.
[25] Davis, B.J. *Phys. Rev. A* **2007,** *76* (4), 043843.
[26] Horowitz, M.; Barad, Y.; Silberberg, Y. *Opt. Lett.* **1997,** *22* (11), 799–801.
[27] Bartels, R.A.; Paul, A.; Green, H.; Kapteyn, H.C.; Murnane, M.M.; Backus, S.; Christov, I.P.; Liu, Y.; Attwood, D.T.; Jacobsen, C. *Science* **2002,** *297,* 376–378.
[28] Born, M.; Wolf, E. *Principles of Optics: Electromagnetic Theory of Propagation, Interference and Diffraction of Light,* 7th (expanded) ed.; Cambridge University Press: Cambridge, UK, 1999.
[29] Arahira, S.; Oshiba, S.; Matsui, Y.; Kunii, T.; Ogawa, Y. *Appl. Phys. Lett.* **1994,** *64* (15), 1917–1919.
[30] Davis, B.J. *Opt. Express* **2007,** *15* (6), 2837–2846.
[31] Magyar, G.; Mandel, L. *Nature* **1963,** *198,* 255–256.
[32] Devrelis, V.; O'Connor, M.; Munch, J. *Appl. Opt.* **1995,** *34,* 5386–5389.
[33] Papadakis, V.M.; Stassinopoulos, A.; Anglos, D.; Anastasiadis, S.H.; Giannelis, E.P.; Papazoglou, D.G. *J. Opt. Soc. Am. B* **2007,** *24* (1), 31–36.
[34] Eberly, J.H.; Wodkiewicz, K. *J. Opt. Soc. Am.* **1977,** *67* (9), 1252–1261.